Pressure-dependent phase transformation of solid helium confined within a nanoporous material

S. Bera,[1] J. Maloney,[1] L. B. Lurio,[1,*] N. Mulders,[2] Z. G. Cheng,[3] M. H. W. Chan,[3] C. A. Burns,[4] and Z. Zhang[5]

[1]*Department of Physics, Northern Illinois University, DeKalb, Illinois 60115, USA*

[2]*Department of Physics and Astronomy, University of Delaware, Newark, Delaware 19716, USA*

[3]*Department of Physics, The Pennsylvania State University, University Park, Pennsylvania 16802, USA*

[4]*Department of Physics, Western Michigan University, Kalamazoo, Michigan 49008, USA*

[5]*Advanced Photon Source, Argonne National Laboratory, Argonne, Illinois 60439, USA*

(Received 13 January 2013; revised manuscript received 7 June 2013; published 26 August 2013)

Transmission x-ray diffraction experiments have been carried out on solid helium grown in porous Vycor glass. Measurements were made at temperatures near 0.7 K and at pressures up to 162 bars. The crystalline phases of solid helium in Vycor are found to differ significantly from the bulk. At pressures from 70 bars through 98 bars the helium is polycrystalline and displays a single size broadened scattering peak. Above 98 bars the peak splits into three close peaks. No higher order peaks are seen at any pressure, indicating significant reduction in intensity due to disorder. A broad peak is present at all pressures, which may indicate the presence of amorphous solid. We tentatively identify the low-pressure phase as bcc and the high-pressure phase as coexistence between bcc and hcp. Size broadening indicates an average grain size of approximately 5 nm, comparable to the Vycor pore size.

DOI: 10.1103/PhysRevB.88.054512 PACS number(s): 67.80.B−, 61.66.Bi, 61.46.Df

I. INTRODUCTION

Solids grown in confined environments often show new and unusual features. For instance, oxygen confined to silica xerogel can show an amorphous phase as well as crystallites much larger than the pore size, indicating that the freezing process can connect across different pores.[1] Ar and Kr in porous Vycor show freezing point suppression, and form a disordered hexagonal close packed (dhcp) structure instead of the face-centered-cubic (fcc) structure found in the bulk.[2] In fact it is likely that most materials can be grown in an amorphous state given the proper nanoscale structure.[3] Moreover, there is a solid-solid phase transition for Ar and Kr in several porous media at about half the melting temperature, which was argued to be due to a transition where the atoms become mobile and are able to move in and out of the pores.[4] Simulations of Ar in disordered porous carbon indicate that the freezing properties depend not only on the properties of the individual pores but also on how they are connected to each other.[5]

Under their own vapor pressure both ^{3}He and ^{4}He remain liquid down to zero temperature. Solidification requires a modest overpressure, 25 bars in the case of ^{4}He and 35 bars for ^{3}He. The low-pressure solid phase of ^{3}He is bcc, whereas ^{4}He forms an hcp crystal, except for a narrow sliver along the melting curve just above the λ line, where the symmetry is bcc.[6] The addition of a small amount of ^{3}He leads to a considerable expansion of the range of the bcc phase in the *P-T* plane.[6,7] The freezing pressure is sensitive to confinement in small pores.[8,9] In porous Vycor glass, with a typical pore diameter of 6–7 nm, the low-temperature freezing pressure can be raised by 12–15 bars. This is believed to be due to the fact that the crystalline solid does not wet the amorphous layer that forms on the pore walls, and that crystallites form by homogeneous nucleation. As already observed by Bittner *et al.*,[9] it is not immediately obvious that when confined on the nanometer scale ^{4}He will have the same crystalline structure as the bulk at corresponding pressure and temperature. From neutron diffraction experiments on ^{4}He in porous gelsil glass with a pore diameter of 7 nm, Wallacher *et al.* conclude that at 38 bars the crystalline component of the solid is in fact in the bcc phase.[10] More recently, Lauter *et al.* reported the observation of coexistence of hcp and bcc with ^{4}He in a 95% porous aerogel, at pressures between 37 and 53.8 bars, with the hcp phase gaining considerably in intensity at 53.8 bars.[11] In a similar aerogel sample, Mulders *et al.* found that at 60 bars ^{4}He is in the hcp phase.[12] Bossy *et al.*[13] studied the structure of helium in a sample of MCM-41, which contained 5 nm pores in a hexagonal pattern with a narrow width distribution. Using neutron scattering they were unable to find any Bragg peaks, indicating a purely amorphous structure. In contrast, ^{4}He crystals which are not confined do not exhibit any measurable amorphous component, although they do show a strong diffuse signal related to the zero-point motion of the atoms.[14] Here, we report our results of x-ray diffraction experiments on ^{4}He confined in porous Vycor, at pressures between 70 and 162 bars.

II. EXPERIMENTAL DETAILS

Vycor is a controlled pore glass made by phase separation of borosilicate glass. When the boron-rich component is leached out, a network of narrow pores is left behind. Transmission electron microscopy reveals channels with a typical size of 30 nm in length and 7 nm in diameter.[15] A nitrogen Brunauer-Emmett-Teller (BET) isotherm confirms this pore size for the Vycor sample used in this experiment. The growth of helium crystals is expected to be limited to roughly the size of the pores, although the helium directly adjacent to the Vycor glass is expected to be disordered.

The experimental sample cell consisted of a 4.0 mm diameter single crystal sapphire tube with a 0.5 mm wall thickness. A single crystal sample chamber was chosen so that it would be straightforward to exclude Bragg scattering from the container through a suitable choice of orientation.

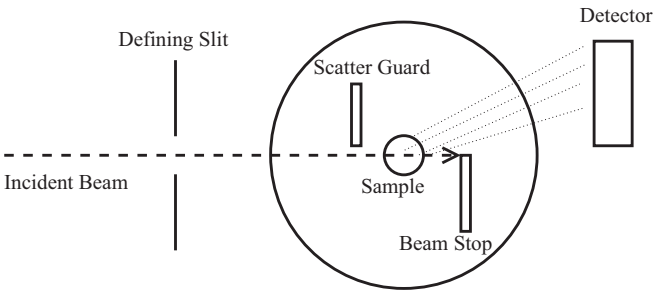

FIG. 1. Schematic drawing of experimental setup.

Inside the sapphire tube was a 4.0 mm diameter Vycor plug. One side of the tube was capped by a titanium membrane that was also part of a capacitive pressure gauge. The other side of the tube was epoxied to a titanium flange that accommodated a high-pressure stainless steel capillary which communicated with a room temperature gas handling system. The cell was mounted in a custom-built dilution refrigerator attached at the base of a pulse-tube refrigerator. The samples were grown using the blocked capillary method. In this method the sample cell is filled with liquid at a pressure and temperature close to the liquid-solid coexistence line such that on cooling the liquid in the pores starts to freeze at the target pressure. The sample cell is then cooled down further at nearly constant pressure to a temperature around 0.7 K

Transmission wide angle x-ray scattering (WAXS) was performed at beam line 33 ID-D of the Advanced Photon Source at Argonne National Laboratory. An x-ray photon energy of 24 keV was employed to obtain as wide a range of scattering vectors through the cryostat window as possible as well as to minimize sample heating due to x-ray absorption. A schematic of the scattering geometry is shown in Fig. 1. The incident beam was defined by $100 \times 100\ \mu m^2$ slits. The entrance and exit windows of the cryostat consisted of a pair of 0.125 mm thick Kapton outer windows and two pairs of 0.025 mm thick double-sided aluminized Mylar windows on the radiation shields. Directly in front of the sample cell was a tantalum scatter guard which blocked the parasitic scattering from the cryostat windows. After passing through the sample cell, the direct beam was intercepted by a beam stop which prevented scattering from the downstream set of cryostat windows. It was not, however, possible to prevent parasitic scattering from the sapphire sample cell itself. The scattered radiation was detected with a MAR 165 CCD detector located 346 mm downstream from the sample cell.

III. RESULTS

The unprocessed scattering from an empty Vycor sample cell is shown in Fig. 2(a) and a sample cell filled with a solid helium sample at 98 bars and at 0.7 K in Fig. 2(b). The helium scattering signal is obscured by the intense background from the Vycor glass in the raw image. After subtracting the background image, however, the helium contribution is clearly visible as shown in Figs. 2(c)–2(i). It was necessary to vary the amplitude of the background by ∼6% to obtain a proper subtraction. The amplitude was chosen by the condition that the background image yield a difference without any features in the region of the Vycor scattering peak. This is a reasonable

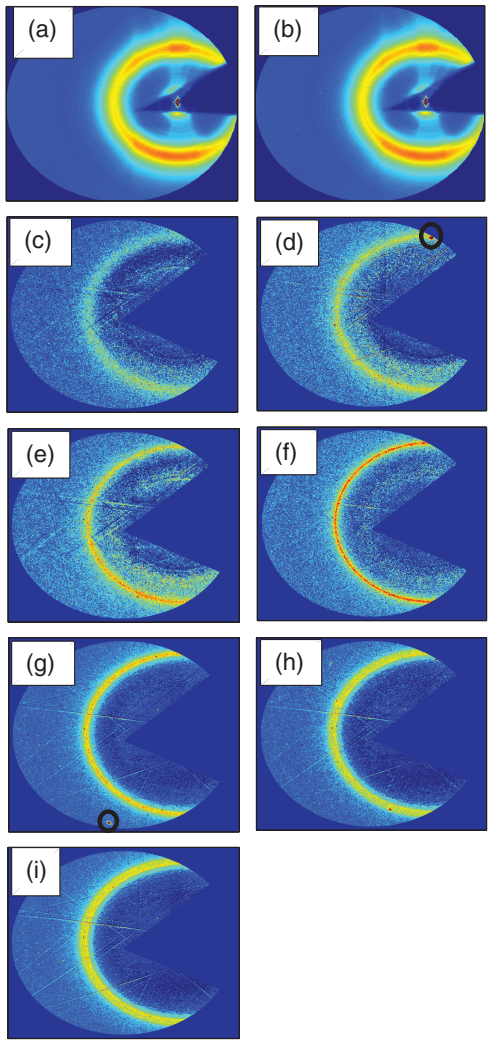

FIG. 2. (Color online) Scattering from (a) Empty Vycor at 0.8 K and (b) solid at 98 bars and 0.8 K. Difference data at (c) 22 bars and 0.25 K (liquid phase) and solid-phase data at (d) 70 bars and 2.0 K, (e) 78 bars and 0.7 K, (f) 98 bars and 0.8 K, (g) 114 bars and 0.7 K, (h) 130 bars and 0.7 K, and (i) 162 bars and 0.5 K. The faint thin straight lines visible in the difference images are Kossel lines from the single crystal sapphire sample cell (Ref. 16).

criteria, since it is not expected that helium should have any features in this region. Figs. 2(c)–2(i) show the helium scattering vs increasing pressure. The diffuse liquid scattering ring seen in the 22 bar data sharpens with increasing pressure and then splits into multiple rings above 130 bars.

More quantitative analysis of the scattering patterns can be made after circularly averaging the images. The data were circularly averaged after masking of the parts of the image where the scattering was blocked, or where Bragg peaks from small crystallites of bulk helium outside the Vycor occurred. An example of such a bulk Bragg peak is shown circled in Fig. 2(d). The dashed red line in Fig. 3 shows the circularly averaged scattering from an empty Vycor cell at 0.8 K and the solid black line shows the scattering from a solid-helium-filled sample at the same temperature. The difference between these two measurements is shown as the solid red line (D) in Fig. 4. This shows a narrow peak at a wave vector of

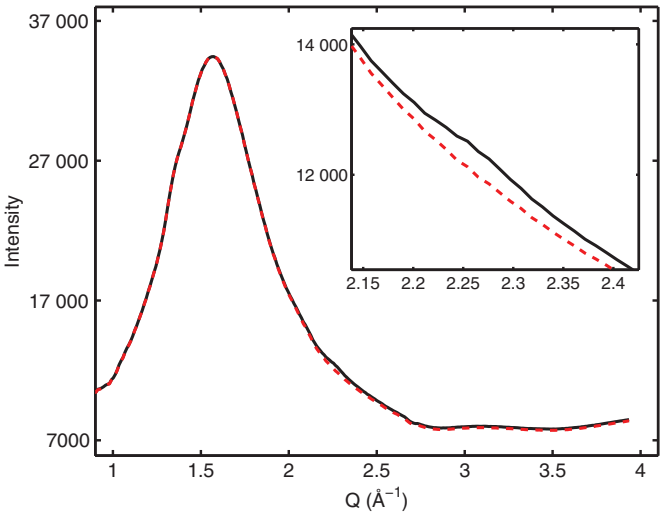

FIG. 3. (Color online) Circularly averaged scattering from empty Vycor (dashed red line) and solid helium filled Vycor at 98 bars and 0.8 K (solid black line). The inset shows a closeup of the region in the vicinity of the helium scattering peak.

$Q \sim 2.3$ Å^{-1}. Here, the wave vector transfer is defined by $Q = (4\pi/\lambda)\sin(\theta)$, and we define 2θ as the scattering angle relative to the incident beam with λ the x-ray wavelength.

A sequence of WAXS measurements were made on solid helium at a range of pressures from 70 bars to 162 bars. Measurements were also made in the liquid phase at 22 bars. The temperature was mainly kept fixed near 0.7 K although some data at slightly different temperatures were also included. Data were processed by subtracting the empty Vycor as described above. The intensity was corrected for geometrical

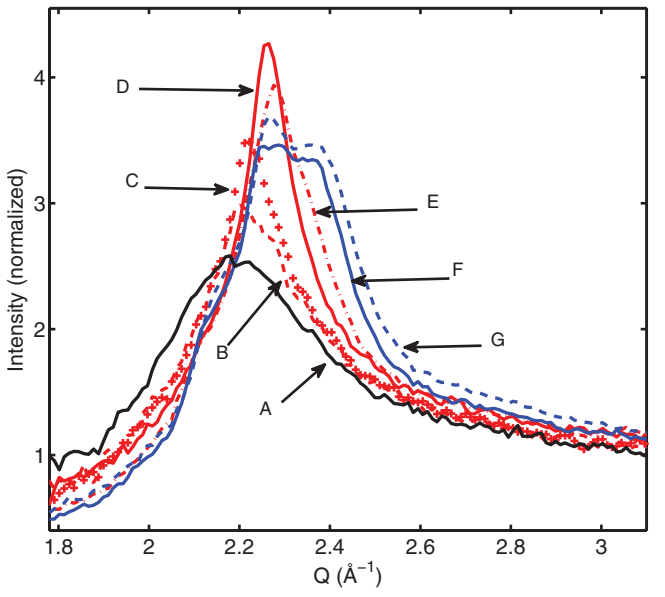

FIG. 4. (Color online) Circularly averaged and background-subtracted scattering: (A) (solid black) 22 bars and 0.25 K liquid phase, (B) (dashed red) 70 bars and 2.0 K solid phase, (C) (red cross) 78 bars and 0.7 K, (D) (solid red) 98 bars and 0.8 K, (E) (red dash-dot) 114 bars and 0.7 K, (F) (solid blue) 130 bars and 0.7 K, (G) (dashed blue) 162 bars and 0.5 K.

factors such as the polarization of the beam, the incline of the detector face relative to the scattered beam, the variation in the distance between the sample and different parts of the detector face, absorption in the sapphire cell, and the variation of efficiency of the camera with angle of incidence. Corrected data were binned by scattering vector Q. The scattering intensity from liquid helium was normalized to unit intensity at $Q = 3.9$ Å^{-1}, and the scattering intensity from solid helium samples was then normalized to the liquid helium intensity at this Q. This normalization allows all the data to be displayed on an identical (although arbitrary) intensity scale

A comparison of the circularly averaged data for all the samples is shown in Fig. 4. As expected, the liquid scattering data display a broad maximum at $Q = 2.18$ Å^{-1}.[17] At pressures below 114 bars the solid displays a single peak near $Q = 2.26$ Å^{-1} which is significantly sharper than the peak in the liquid. As the pressure is increased the solid peak gains in intensity and moves to larger Q indicating that the fraction of crystalline helium is increasing and that the solid is compressing. For pressures of 114 bars and above the peak begins to broaden again and split indicating two-phase coexistence. No higher order peaks beyond $Q = 2.6$ Å^{-1} are observed at any pressure. The measured data also show a significant background at higher Q values. We interpret that this background is due to a combination of Compton scattering and diffuse scattering. The diffuse component is analogous to what is usually referred to as thermal diffuse scattering, although in the case of helium, the zero-point motion of the atoms (up to ~25% of the lattice spacing for ^{4}He) is the main contributor. The diffuse scattering is comparable to what would be expected from bulk helium crystals, as will be discussed in the next section. The Bragg peaks of the solid, while narrower than the liquid, are still quite broad. This width is not due to resolution effects, which contribute less than 0.03 Å^{-1} to the width while we find typical widths of order 0.1 Å^{-1}.

It is not possible to assign a definitive crystal structure based on only a single peak. Even in the case of the higher pressure phase where the peak splits into three we lack any higher order peaks which would allow us to definitively confirm the structure. Instead we have examined the most likely crystal structures for helium based on the observed phases of bulk helium in this temperature and pressure range. These are body-centered cubic (bcc) and hexagonal close packed (hcp). We have also explored the possibility of face-centered cubic (fcc), as it is closely related to the hcp phase. In order to understand the lack of higher order peaks, we have considered two separate causes; the first is attenuation of the peak amplitude due to the Debye-Waller factor, and the second is the possibility of lattice defects.

Figure 5 displays the single peak observed at 98 bars and compares it with the expected peak positions for hcp, fcc, and bcc phases. The presence of only a single peak is incompatible with either fcc or hcp as shown in Fig. 5. Hence we assume that the single peak at 98 bars is due to the bcc (110) Bragg peak. The next two higher order peaks from the bcc phase should be the (200) and (112) peaks which should appear at $Q = 3.19$ Å^{-1} and $Q = 3.91$ Å^{-1}, respectively. Neither of these is observed. To try to understand this we have calculated the expected higher order peak intensities based on the structure factor multiplicity and Debye-Waller factor. The Debye-Waller

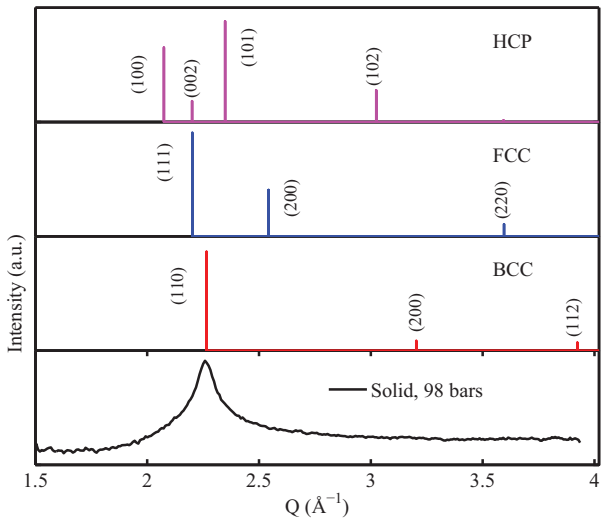

FIG. 5. (Color online) Diffraction pattern from 98 bars solid sample with different possible crystal structures. The best matching structure is the bcc.

factor calculation was made by estimating an effective Debye temperature for each sample based on its molar volume using the data of Gardner *et al.*[18] The Debye Waller factor attenuates each peak by a factor of $\exp(-\langle u^2\rangle Q^2)$. The value of $\langle u^2\rangle$ as a function of the Debye temperature was obtained by using the data of Arms *et al.*[19] with our estimated Debye temperatures. Note, however, that both Gardner *et al.* and Arms *et al.* give data for the hcp phase, while most of our data is for what we believe to be the bcc phase. Our calculations assume that the Debye Waller factor for the bcc phase will be comparable.

The theoretical peak heights shown in Fig. 5 are corrected for the Debye-Waller factor. While the intensity of the (200) peak is significantly reduced it would still be expected to be visible in the measured scattering. This indicates that the crystal is more disordered than would be expected on the basis of zero-point motion alone. We also note that the neutron scattering results of solid helium in mesoporous glass, similar to Vycor, also showed only one peak.[10]

At higher pressures the central peak splits into multiple peaks. We interpret this to be coexistence between bcc and hcp phases. In order to quantitatively analyze the higher pressure data, the peaks were fit to a model for the scattering. At pressures below 114 bars the peak was modeled as a bcc peak. The structure factors and multiplicities for all the peaks were included and each order peak was multiplied by an appropriate Debye-Waller factor as described above. In addition, the peaks were broadened by a Gaussian function in order to model the effects of finite grain size. At higher pressures, the peaks were fitted to a superposition of bcc and hcp phases. The Gaussian widths were constrained to be identical for each peak within a given phase, but the two phases were allowed to have differing widths. The modeled fits include the higher order peaks which are missing in the data. In this respect, these models do not do a good job of describing the data in the high-Q range.

There is a significant contribution from diffuse scattering which also needs to be included in the fits. In order to model the diffuse scattering we used a measurement of diffuse scattering from a single crystal of helium in the hcp phase measured at

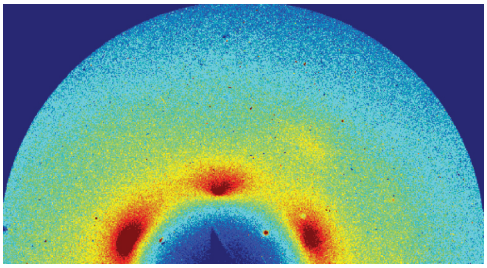

FIG. 6. (Color online) Diffuse scattering from single crystal of solid helium grown at 2 K and 28 bars. The triangular shadow near the center of the scattering pattern is due to the beam stop. The crystal was not aligned to a Bragg peak but beyond this the orientation of the crystal was not known.

28 bars and 2 K. The crystal was aligned so as to not satisfy the Bragg condition, providing a measure of only the diffuse scattering from bulk helium. Note that this measurement should also include the Compton scattering contribution. Figure 6 shows an image of scattering from a solid helium crystal grown at 28 bars and 2 K. This measurement was made during a different experimental run on a crystal grown in a copper sample cell with single crystal sapphire windows. The sapphire window background measured from an empty cell was subtracted from the single-crystal data. The crystal was not aligned to the Bragg condition, but the image shows clearly enhanced scattering in a hexagonally symmetric pattern near the Bragg conditions as is expected for diffuse scattering from single crystals.[20] To obtain an estimate of the solid diffuse background we took a cut through the scattering pattern midway between the higher intensity regions close to Bragg peaks. This diffuse function, $S_d(Q)$, was then used to fit the diffuse scattering from the helium in Vycor measurements. The diffuse scattering from the single crystal will most likely depend on pressure, temperature, and crystal phase, so there is no reason to believe that the single-crystal diffuse will be an exact match to the diffuse scattering within the Vycor. However, the shape of this function does do a reasonable job of approximating the shape of the measured diffuse when it is allowed to be scaled and stretched. Specifically, we modified the measured single-crystal diffuse with two adjustable parameters: an amplitude A and a stretching ratio r, so that $S_{\rm fit}(Q) = AS_d(Qr)$. These two parameters were then allowed to vary to provide the best fit to the data. The single-crystal diffuse scattering used in each of the fits are shown as the dashed green lines in Fig. 7. Inclusion of the single-crystal diffuse did not, however, prove sufficient to model the measured diffuse scattering. In addition, the fits included a broad Gaussian component near the vicinity of the liquid structure factor peak. The amplitude, width, and position of this broad Gaussian were all allowed to vary. A nonlinear least-squares fitting routine was then used to fit the data to the sum of these four components, the bcc peaks, the hcp peaks, the bulk diffuse, and the additional Gaussian. Taken together, the diffuse background and Gaussian peak could either represent the diffuse scattering from the crystalline phase or, alternately, scattering from a separate amorphous phase.

Figure 7 shows the best-fit results for all the measured pressures. The contribution to the fit from each of the four components described above is portrayed separately. For the

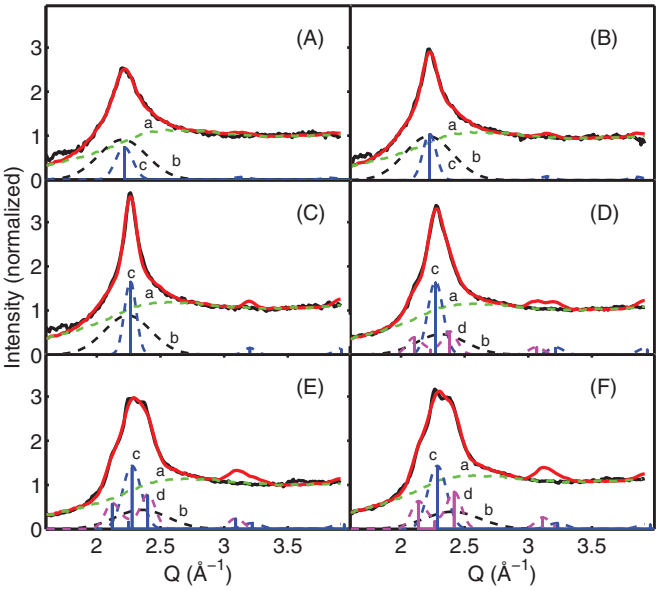

FIG. 7. (Color online) Fits to scattering from solid He as a function of pressure. The measured data are shown as the solid black lines. The fits are shown as the solid red lines. The fits are also decomposed into their four component parts with (a) (dashed green) the solid diffuse, (b) (dashed black) the broad Gaussian, (c) (dashed blue) the bcc peaks, and (d) (dashed magenta) the hcp peaks. The six panels show (A) 70 bars and 2.0 K, (B) 78 bars and 0.7 K, (C) 98 bars and 0.8 K, (D) 114 bars and 0.7 K, (E) 130 bars and 0.7 K, and (F) 162 bars and 0.5 K.

three lowest pressures, the hcp peaks are not required for the fit. For pressures of 114 bars and above a transition occurs initially to a broadened first peak which resolves into a clearly defined splitting for pressures of 130 bars and above. We interpret the middle of these three peaks to be a superposition of the hcp (002) peak and the bcc (110) peak, since the hcp (002) by itself is inconsistent with the measured peak intensity ratios.

The crystallite sizes can be obtained from the width of the peaks using the Scherrer equation $D = K\lambda/L\cos(\theta)$, where K is the shape factor of order 1 and L is the line broadening at

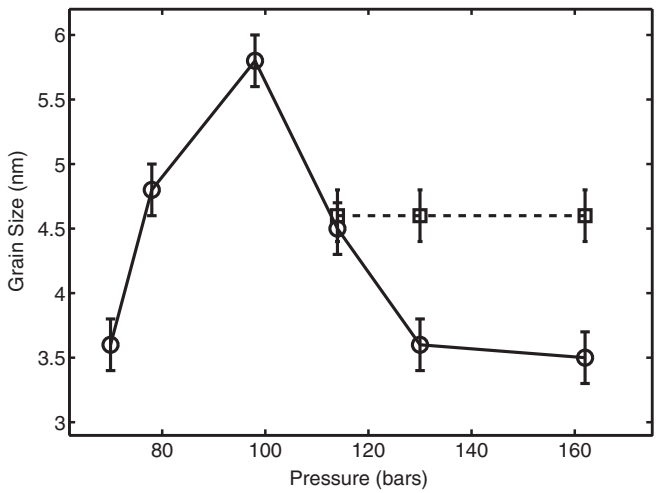

FIG. 8. Change of bcc (circles connected by solid line) and hcp (square connected by dashed line) grain size vs pressure.

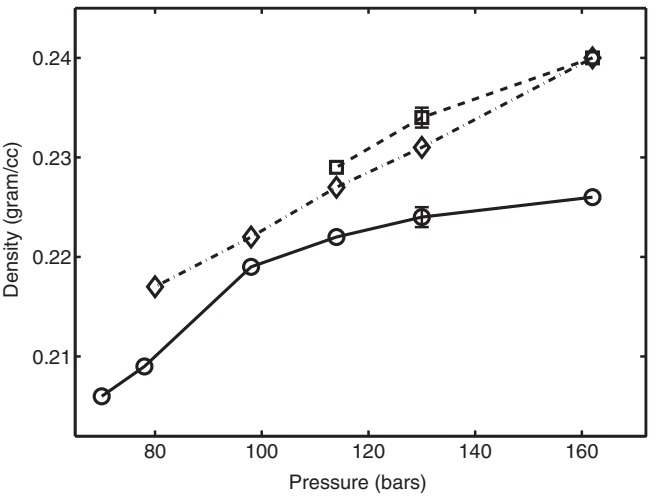

FIG. 9. Change of bcc (circles connected by solid line) and hcp (squares connected by dashed line) density vs pressure. For comparison, we also plot the variation of the bulk hcp density with pressure (diamonds connected by dashed-dotted line).

half the maximum peak intensity. These sizes are displayed as a function of pressure in Fig. 8. The average grain size of the bcc phase initially increases with pressure and then decreases above 98 bars. The grain size in the hcp phase remains nearly independent of pressure as shown by the dashed line in Fig. 8.

The crystallite density can be found from positions of the peaks if one assumes a specific crystal phase. Inferred densities for the bcc and hcp phases are shown in Fig. 9. Within the bcc phase the density increases with pressure but the compressibility begins to level off for pressures where the hcp phase coexists with the bcc. The hcp crystal density shows a monotonic increase with pressure for the three pressure values that were measured. Along with the measured data, Fig. 9 also shows the density of bulk solid helium measured along the liquid-solid coexistence line at the same pressures as the measured data. Bulk solid helium densities were obtained from Wilks.[21] The density of the hcp phase in Vycor is found

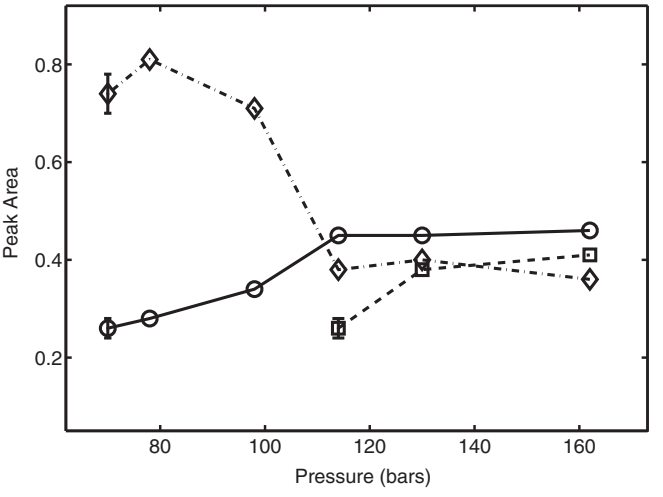

FIG. 10. Change of bcc (circles connected by solid line), hcp (squares connected by dashed line), and amorphous (diamonds connected by dashed-dotted line) peak areas vs pressure.

to be within 1% of the expected bulk value at the measured pressures. One can also attempt to quantify the amount of material within each phase by considering the integral of the areas under the peaks of the diffraction data. Such an analysis is not strictly accurate, however, since the peak area is only proportional to the volume of material if the crystallite size does not change with pressure. Figure 10 displays the variation of the integral under the area of the peaks within each of the two phases as a function of pressure. As the pressure is increased the bcc peak areas initially grow until the entry of the hcp phase. After that point the hcp peak areas grow while the bcc peak area remains approximately constant. Figure 10 also shows the area under the Gaussian peak used to represent the amorphous material or bulk diffuse scattering. This peak area is approximately constant at low pressure. When the pressure is raised to 114 bars it shows a sharp decrease and then remains relatively constant for further increasing pressure.

IV. DISCUSSION

It is interesting to compare the present results with those of Bossy *et al.*[13] who measured helium in MCM-41, a porous glass with a smaller pore diameter of 5 nm. Those investigators also see only a single peak, but interpret their measurements in terms of an amorphous phase with only local order. This result is similar to our lower pressure data. For example, at 70 bars we find that the crystallite size is only around 3.5, much smaller than our 7 nm pore size. With increasing pressure, however, we see indications of the growth of larger scale crystals. In our case the crystallite size increases continuously with pressure until it reaches a size of 6 nm, which is consistent with what would be expected for a crystallite in a 7 nm pore covered by a dead layer of helium coating the silica. It is on the basis of these large correlation lengths that we claim a bcc phase as opposed to the amorphous solid claimed by Bossy *et al*. Our observed variation of the degree of crystallinity with pressure is also qualitatively consistent with the theoretical work of Coasne *et al*.,[5] who find that classical fluids confined to nanopores become gradually more ordered as the temperature is lowered deeper into the region where the bulk is a solid. In our case pressure would play a role similar to that of temperature. The differences between our observations and those of Bossy *et al.* could then be explained as due to the differences in pressure between the two measurements. The highest pressure reported by their measurements was 61 bars, while our lowest pressure was 70 bars. Another explanation is that the difference between the two measurements is due to the differences in pore size. This is supported by theoretical models by Sliwinska-Bartosky *et al*.,[22] who find that for pore diameters smaller than 20 σ, where σ is the atomic diameter, one should obtain an amorphous solid. For ^{4}He, $\sigma \sim 2.6$ Å provides a transition length scale of around 5 nm. This would imply that our samples should show crystallinity, while those of Bossy *et al*. would not.

Our finding of a phase transition from bcc to hcp at around 114 bars has not been previously observed. It is interesting that this phase transition occurs at or near the same pressure where the inferred crystallite size for the bcc phase equals the Vycor pore size. This implies that the bcc phase grows until it reaches the size of the pores, and then begins to transform to the hcp phase. The inferred crystallite size of the hcp phase is 4.6 nm, which is somewhat smaller than the Vycor pore size. This implies that the hcp is likely in coexistence with an amorphous phase which coats the walls of the pores, or alternately the pores consist of an inner core of hcp surrounded by a bcc shell. As with the case for the bcc phase, the hcp does not show any higher order peaks, even though the signal to noise ratio of the data should be sufficiently good to resolve these if they were present. One plausible explanation for the lack of higher order hcp peaks would be the presence of stacking faults along the [111] direction, which is the direction normal to the hexagonal planes. Stacking faults were also seen by Brown *et al*.[2] for rare gas solids in porous media. It seems likely that the interface with the Vycor glass could induce a high density of stacking faults during the crystallization within the pores. Stacking faults should not effect the observed (100) and (002) peaks, but should modify the (101) peak. However, since the hcp (101) overlays the bcc (110) its absence or modification would be difficult to verify. Completely random stacking is expected to produce Bragg rods between the peaks as was discussed by Wallacher *et al*.[10] However, these Bragg rods would be difficult to see in a randomly oriented powder. It is hard to draw conclusions from the other missing peaks in the hcp phase, as their intensities would be too small to observe due to the Debye-Waller factor. Even in the absence of high order peaks, our claim that this is a crystalline hcp phase is supported by a number of other factors. First, the inferred grain size is comparable to the pore size. Second, there are three peaks whose positions are correct for the hcp phase. While the amplitude ratio of the central of the three peaks is incorrect, we attribute this to superposition of hcp and bcc phases, an interpretation which is supported by the decrease in the central peak amplitude with pressure. Third, the inferred molar volume from the hcp peak positions agrees to within 1% with the molar volume of bulk ^{4}He at the same pressure along the solid-liquid coexistence line. Indeed, since the hcp phase is the dominant phase for bulk ^{4}He it requires some explanation as to why the bcc phase is present at all. One possible explanation is that the presence of defects created by incommensurate packing constraints at the Vycor-helium boundary would impose less energy cost on the bcc phase than the hcp. This could also lead to two-phase coexistence with the bcc fully occupying the smaller pores and partially occupying the larger pores. It is not surprising that higher pressures favor the hcp, since this phase has the lower molar volume.

One can imagine two plausible explanations for the observed two-phase coexistence between hcp and bcc. Since the Vycor pores are not all identical, some pore environments favor the bcc and some pore environments favor the hcp. Presumably, the larger pores would favor the hcp since the effect of defects induced from the interfaces would be smaller in this case. An alternative explanation is that there is a layered crystal phase within each pore, with a bcc phase nearest the walls, and an hcp phase within the core. As mentioned earlier, this would be consistent with the smaller inferred crystallite size from the hcp peak widths.

Finally, an important issue is to what extent the current data support the interpretation of a region of amorphous ^{4}He. Indeed, the original motivation for the present work was that the presence of amorphous solid helium was posited as an

explanation for the nonclassical rotational inertial (NCRI) observed by Kim and Chan.[23] This explanation has become less compelling since NCRI now appears to be accounted for in terms of sheer modulus stiffening.[24] While earlier experiments have claimed to observe amorphous helium in porous materials[13] these results have been called into question by the recent neutron scattering results of Mukharsky *et al*.[14] They report inelastic neutron scattering measurements which imply that all the observed diffuse scattering is dynamic, and hence does not result from an amorphous solid. Further they find that the diffuse scattering of the crystalline phase is nearly identical to that from the liquid phase.

In our analysis we have chosen to break the diffuse scattering down into two components, a broad diffuse background, which we attribute to the solid phase, and which we obtain from a cut through the single-crystal diffuse along a direction away from the influence of Bragg peaks, and a single broad Gaussian peak which could result from either an amorphous solid or alternately from enhanced diffuse scattering near the Bragg peaks. An interesting result of the present work is that the Gaussian peak contribution to the diffuse scattering decreases with increasing pressure. This is certainly not what would be expected from diffuse scattering which resembled that of the liquid, since the liquid helium peak intensity is known to increase with pressure.[17] We also find the coincidence of the diffuse scattering from the liquid and solid found by Mukharsky *et al*. somewhat puzzling, since our own measurements from single-crystal helium indicate that the diffuse scattering from the solid differs clearly from a liquid in that it is has angular dependence. While it may be possible that the single-crystal diffuse scattering resembles the liquid after angular averaging, we can see no obvious reason why it should do so. Nevertheless, we cannot rule out the possibility that we are seeing diffuse scattering from a single crystal which happens to show a broad peak which decreases with increasing pressure. We find more likely, however, the alternative explanation that the broad peak seen in the diffuse scattering data results from an amorphous fraction which decreases with increasing pressure. A more detailed theoretical analysis of the pressure dependence of the diffuse scattering from a single crystal could help more clearly distinguish these two possibilities.

In conclusion, we propose the following scenario for the growth of the solid in porous Vycor with pressure. At pressures below 70 bars, much of the solid is either in an amorphous state or filled with bcc crystal that has a correlation length significantly smaller than the pore size. The bcc phase grows with increasing pressure until the pores are filled with bcc, except for an amorphous layer at the surface. This occurs in the vicinity of 114 bars. Above 114 bars, the bcc filled pores convert to hcp; this is either a partial conversion with some pores remaining bcc and some converting to hcp, or the pores are layered, with bcc near the walls and hcp in the core. It is also expected that amorphous ^{4}He remains directly adjacent to the silica in all pores. Due to the confinement in the silica all the single-crystal phases are highly defective, which prevents the observation of higher order peaks.

ACKNOWLEDGMENTS

We would like to acknowledge support from the National Science Foundation Division of Materials Research, Grants No. DMR-0804591, No. DMR-0804725, No. DMR-1103159, and No. DMR-0804643. Use of the Advanced Photon Source was supported by the US Department of Energy, Office of Science, Office of Basic Energy Sciences, under Contract No. DE-AC02-06CH11357.

*Corresponding author: llurio@niu.edu

[1] B. Schirato, M. P. Fang, P. E. Sokol, and S. Komarneni, Science **267**, 369 (1995).
[2] D. W. Brown, P. E. Sokol, and S. N. Ehrlich, Phys. Rev. Lett. **81**, 1019 (1998).
[3] K. Nishio, W. Shinoda, T. Morishita, and M. Mikami, J. Chem. Phys. **122**, 124715 (2005).
[4] D. E. Silva, P. E. Sokol, and S. N. Ehrlich, Phys. Rev. Lett. **88**, 155701 (2002).
[5] B. Coasne, S. K. Jain, and K. E. Gubbins, Phys. Rev. Lett. **97**, 105702 (2006).
[6] J. H. Vignos and H. A. Fairbank, Phys. Rev. **147**, 185 (1996).
[7] D. S. Miyoshi, R. M. Cotts, A. S. Greenberg, and R. C. Richardson, Phys. Rev. A **2**, 870 (1970).
[8] L.-Z. Cao, D. F. Brewer, C. Girit, E. N. Smith, and J. D. Reppy, Phys. Rev. B **33**, 106 (1986).
[9] D. N. Bittner and E. D. Adams, J. Low Temp. Phys. **97**, 519 (1994).
[10] D. Wallacher, M. Rheinstaedter, T. Hansen, and K. Knorr, J. Low Temp. Phys. **138**, 516 (2005).
[11] H. V. Lauter, V. Apaja, I. Kalinin, E. Kats, M. Koza, E. Krotscheck, V. V. Lauter, and A. V. Puchkov, Phys. Rev. Lett. **107**, 265301 (2011).
[12] N. Mulders, J. T. West, M. H. W. Chan, C. N. Kodituwakku, C. A. Burns, and L. B. Lurio, Phys. Rev. Lett. **101**, 165303 (2008).
[13] J. Bossy, T. Hansen, and H. R. Glyde, Phys. Rev. B **81**, 184507 (2010).
[14] Y. Mukharsky, A. Braslau, J. Bossy, T. Hansen, and M. M. Koza, Europhys. Lett. **101**, 26002 (2013).
[15] P. Levitz, G. Ehret, S. K. Sinha, and J. M. Drake, J. Chem. Phys. **95**, 8 (1991).
[16] R. W. James, *The Optical Principles of X-Rays* (Ox Bow Press, Woodbridge, CT, 1982).
[17] F. H. Wirth and R. B. Hallock, Phys. Rev. B **35**, 89 (1987).
[18] W. R. Gardner, J. K. Hoffer, and N. E. Phillips, Phys. Rev. A **7**, 1029 (1973).
[19] D. A. Arms, R. S. Shah, and R. O. Simmons, Phys. Rev. B **67**, 094303 (2003).
[20] B. E. Warren, *X-Ray Diffraction* (Addison-Wesley, Reading, MA, 1969; reprinted by Dover Publications, New York, 1990).
[21] J. Wilks, *The Properties of Liquid and Solid Helium* (Oxford University Press, Oxford, 1967).
[22] M. Sliwinska-Bartkowiak, G. Dudziak, R. Sikorski, R. Gras, R. Radhakrishnan, and K. E. Gubbins, J. Chem. Phys. **114**, 950 (2001).
[23] E. Kim and M. H. W. Chan, Nature (London) **427**, 225 (2004).
[24] D. Y. Kim and M. H. W. Chan, Phys. Rev. Lett. **109**, 155301 (2012).